DALTON
FULL PAPER

Electronic structure of chalcogenols: photoelectron spectroscopic and theoretical studies of tris(trimethylsilyl)silyl chalcogenols

Jessima M. Timberlake,[a] Jennifer Green,[a] Victor Christou[a] and John Arnold[b]

[a] *Inorganic Chemistry Laboratory, University of Oxford, South Parks Road, Oxford, UK OX1 3QR*
[b] *Department of Chemistry, University of California, Berkeley, California 94720, USA*

Received 10th September 1998, Accepted 15th October 1998

The photoelectron spectra (He I and He II) have been reported for the homologous series of tris(trimethylsilyl)silyl chalcogenols $(Me_3Si)_3SiEH$ (E = O, S, Se or Te) and assigned on the basis of predictions from density functional theory (DFT) calculations. The DFT calculations indicated that the chalcogenol HOMO is a π-type orbital located essentially on the silicon atoms for the lighter chalcogenols, whilst it is located entirely on the chalcogen for selenol and tellurol. DFT was used to predict the H–E–Si bond angle in the idealised species $HESi(SiH_3)_3$. The trends seen, on descending the group, are broadly similar to those obtained for H_2E, but are complicated by mixing of silicon orbitals with those of E. The results of these studies are used to rationalise the observed behaviour of some transition metal chalcogenolate complexes, in particular the facile Te–Si bond cleavage reactions which produce terminal tellurides for the early d-block metals.

Introduction

Compounds containing metal–chalcogenide bonds have aroused considerable interest in recent years.[1,2] The lighter elements are of interest primarily because of their biological significance whereas the heavier homologues are important constituents in thin film semiconducting materials. However, in contrast to compounds of oxygen and sulfur, which are very familiar and whose complexes are well documented,[3–8] the organic compounds of selenium and tellurium are much less frequently encountered and their metal complexes were, until the last decade, extremely scarce.[9–11] Recent studies with the bulky tris(trimethylsilyl)silyl fragment however have yielded several interesting main group,[12–15] transition metal[16–23] and lanthanide complexes,[24–26] and the first example of a tellurol stable at room temperature, $(Me_3Si)_3SiTeH$.[27,28] Not only does the bulky silyl fragment engender unprecedented stability to the heavy chalcogen–heteroatom bond, but it also provides clean pathways for the subsequent reactivity of the metal chalcogenolate complex, including the chalcogenolate to chalcogenide transformation, eqn. (1).[16,29]

$$L_nM(TeR)_2 \longrightarrow L_nM{=}Te + R{-}Te{-}R \qquad (1)$$

Since molecular species may be used as precursors for technologically important solids such as II/VI materials,[30,31] detailed knowledge of the factors governing reactions similar to that shown in eqn. (1) is vitally important for the development of appropriate reagents. While recent mechanistic studies have begun to shed light on this chalcogenolate-to-chalcogenide transformation, there still is much to be learned.[29] Since there have been no systematic electronic investigations on systems of this kind to date, we thought it timely to investigate the electronic properties of the homologous series $(Me_3Si)_3SiEH$ (E = O **1**, S **2**, Se **3** or Te **4**) to improve our understanding of the reactivity of these species. Herein we report on the UV-PES of these species combined with a theoretical study of the idealised species $(H_3Si)_3SiEH$ using density functional theory (DFT).

Experimental

The compounds **1**–**4** were synthesized and purified according to the literature procedure.[27,32,33]

The He I and He II photoelectron (PE) spectra of compounds **1**–**4** were obtained using a PES Laboratories 0078 PE spectrometer interfaced with an Atari microprocessor, and calibrated using N_2, Xe and He. A sample of **1** was sufficiently volatile to be held outside the spectrometer and measured at room temperature. For **2**, **3** and **4** the sample was raised to a temperature of 40 °C inside the spectrometer.

Computational details

All density functional calculations were carried out using GAUSSIAN 94.[34] The basis set employed was LanL2DZ. The three density functional methods used are defined as follows: (1) BLYP which combines the 1988 Becke exchange functional[35] which includes Slater exchange[36] along with corrections involving the gradient of the density, and the correlation functional of Lee *et al.*[37] which includes both local and non-local terms; (2) LSDA Local Spin Density Approximation, which uses the Slater exchange functional[36] and the correlation function of Vosko *et al.*[38] and is also known as the SVWN method; (3) B3LYP Becke's 3 parameter hybrid[39] method using the LYP correlation functional.[37] The calculations performed are summarised in Table 1.

Results and discussion

The He I PE spectra of compounds **1**–**4** are shown in Fig. 1. Vertical ionisation energies (IE) are given in Table 2. The He II spectra were also recorded. Though the count rates on the low energy bands were low, no significant intensity changes were observed so the spectra are not given here.

Each of the four sets of PE spectra shows at least four bands. Bands **C** and **E** remain fairly constant in ionisation energy throughout the series but other bands change IE significantly and band region **A** splits into two as the series is descended. It is therefore assumed that for compound **1** the first band consists

Table 1 Calculations performed using GAUSSIAN 94 on compounds **5**–**8**

Molecule	Calculation type
$HOSi(SiMe_3)_3$, analogue used $HOSi(SiH_3)_3$ **5**	Full geometry optimisations LSDA, BLYP, B3LYP Single point energy calculations LSDA at 80, 100, 120, 140, 160, 180°
$HSSi(SiMe_3)_3$, analogue used $HSSi(SiH_3)_3$ **6**	Full geometry optimisations LSDA, BLYP, B3LYP Single point energy calculations LSDA at 80, 100, 120, 140, 160, 180°
$HSeSi(SiMe_3)_3$, analogue used $HSeSi(SiH_3)_3$ **7**	Full geometry optimisations LSDA Single point energy calculations LSDA at 80, 100, 120, 140, 160, 180°
$HTeSi(SiMe_3)_3$, analogue used $HTeSi(SiH_3)_3$ **8**	Full geometry optimisations LSDA Single point energy calculations LSDA at 80, 100, 120, 140, 160, 180°

of two almost coincident bands, **A1** and **A2**. These then separate in energy as E is varied. Consequently there are at least three ionisations which vary with the changing identity of the chalcogen, E.

For all four spectra a broad band **E** lies between 12 and 16 eV, with a maximum around 14 eV. This is analogous to a band found in the PE spectrum of tetramethylsilane, and may be assigned to ionisations from the C–H bonds.[40] Band **C**, centred around 10.4 eV, is in the characteristic region for Si–C ionisations.[40]

The photoelectron spectra for the simpler H_2E series have been studied by Potts and Price.[41] The chalcogenols are analogous to these compounds, where one of the H ligands in H_2E has been replaced by the ligand $Si(SiMe_3)_3$. In Fig. 2 the vertical IE found for H_2E are mapped together with average ionisation energies associated with the photoelectron spectra of the trimethylsilane ligands, and carbon–silicon and silicon–silicon bonds, which have been estimated from various existing spectra of related compounds.[40–45] Examination of Fig. 2 suggests that bands $\mathbf{A_1}$, $\mathbf{A_2}$ and **B** and **D** are likely to be associated with Si–Si and E ionisations.

Further assignment is possible with the assistance of density functional calculations. Though there is no exact equivalence between Kohn–Sham one electron energies (the DFT equivalent of an orbital energy) and the corresponding ionisation energy, it has been found that the former gave a good representation of the IE pattern and its variation in a closely related set of compounds.[46] Owing to the size of compounds **1**–**4**, density functional calculations were carried out on analogues of these compounds, $HXSi(SiH_3)_3$ (X = O **5**, S **6**, Se **7** or Te **8**), which used a simplified version of the $Si(SiMe_3)_3$ ligand. Occurrence of Si–Si ionisations in the low IE region meant it was essential to retain these in the model. As reported for PES of similar compounds, Si–H ionisations lie just above Si–C ionisations in IE.[40,42–45] The distance of the methyl groups in the ligand from the chalcogens means that there is no direct interaction with the chalcogen, and the similarity of ionisation energies suggests that they occur in a similar position in the one electron energy manifold. Therefore it may be assumed that the model series is a good approximation of the electronic environment of the complexes.

As no structural data exist for these compounds, the geometries were optimised by calculation. Orbital energies were also calculated for a range of geometries for the chalcogenols, by varying the Si–E–H angle from 180 to 80°. The effect of varying the angle on these energies can be seen in the Walsh diagrams in Fig. 3, which show the variation for the first six orbitals (HOMO uppermost). These are shown as it is the frontier orbitals that are expected to exhibit the greatest energy diversity. The optimised Si–E–H angles are given in Table 3. Each of

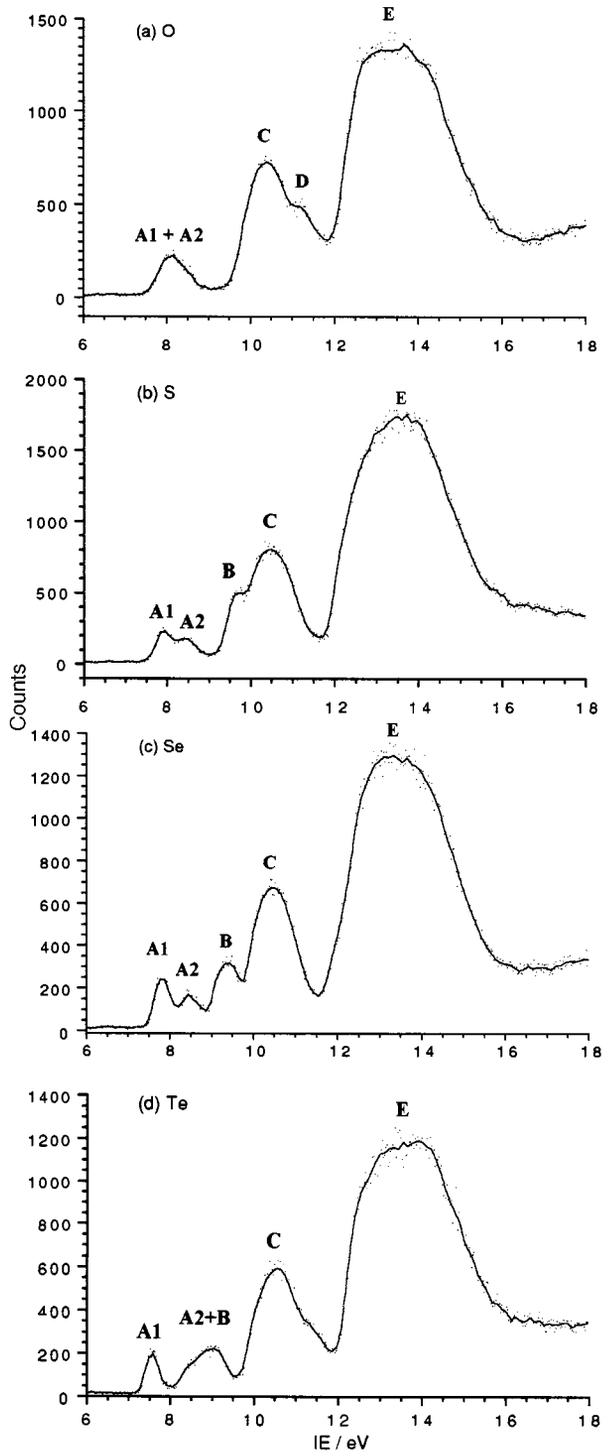

Fig. 1 Low energy range He I PE spectra of compounds **1**–**4**.

Table 2 Vertical IE (eV) of the compounds **1**–**4**

	1		2		3		4
A1 + **A2**	8.138	**A1**	7.914	**A1**	7.795	**A1**	7.536
		A2	8.478	**A2**	8.512	**A2**	8.5 (sh)
		B	9.665	**B**	9.354	**B**	9.022
C	10.367	**C**	10.450	**C**	10.465	**C**	10.552
D	11.223						
E	13.340	**E**	13.430	**E**	13.263	**E**	13.541

the three different methods used to optimise the H–E–Si bond angle of **5** and **6** gave very similar predictions.

From the optimised structures, oxygen was found to have a much larger Si–E–H angle than its congeners due to the different relative stabilisation of the orbitals caused by bending the

molecule. The stabilisation of the second orbital shown on the Walsh diagram is much greater on reducing the angle for the heavier chalcogens than it is for oxygen. The uppermost π orbitals, which are degenerate when the structure is linear, are both stabilised to differing extents by decreasing the angle in question, partially due to reduced repulsion within the molecule as electron density is removed from the chalcogen and supported by the protons, whereas for H_2E only the $2a_1$ orbital is stabilised.

The first ionisation energies seen in the H_2E PE spectra vary widely as the group is descended. This is certainly not true of the chalcogenol series, as seen in Fig. 1; here the first ionisation energies vary only by *ca.* 0.6 eV, compared to *ca.* 3.5 eV for the H_2E series. We infer from this that the frontier orbitals of the silyl series are more complicated than those of the hydrides.

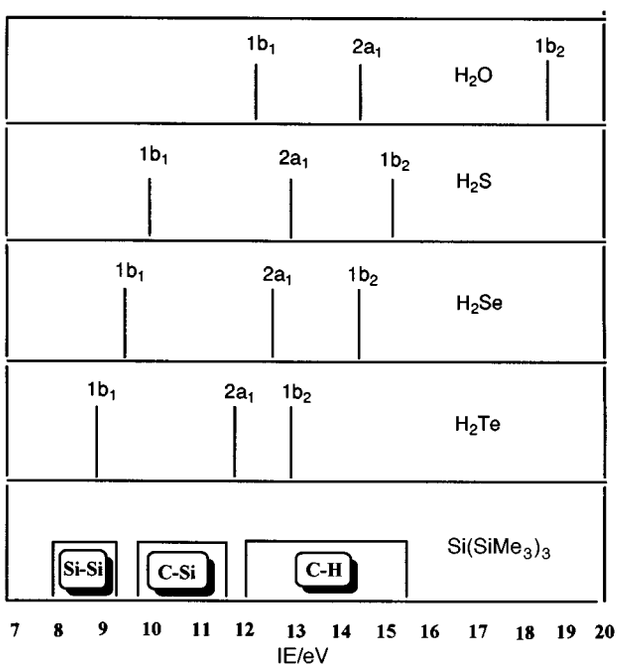

Fig. 2 Diagram indicating the vertical IE of H_2E PE spectra and the IE range of bands expected for the $Si(SiMe_3)_3$ ligand.

Representations of the two highest occupied orbitals are shown in Fig. 4. The frontier orbitals of the geometrically optimised alcohol are indeed different from those of the rest of the series. The HOMO of compound **8** is a p_π orbital almost entirely localised on Te. The HOMO of **5** involves mainly Si–Si interactions instead of the mainly chalcogenic interactions seen in the HOMOs of the heavier congeners. It has an antibonding interaction with the oxygen p_π orbital.

The second occupied molecular orbital (SOMO) of compound **5** is also principally Si–Si localised but changes progressively as the group is descended until at Te it shows Te–Si bonding character. The Walsh diagrams show that the gap between the HOMO and SOMO increases down the group. This is consistent with the SOMO gaining bonding character, and with the trends found in bands **A1** and **A2** in the PE spectra. Bands **A1** and **A2** can be assigned on this basis to the HOMO and SOMO respectively.

The reason for this change in the character of the frontier orbitals lies with the electronegativity of the chalcogen. As the group is descended the chalcogen becomes less electronegative. As a result the mainly chalcogen character molecular orbitals are held less tightly in the molecule and steadily increase in energy. The oxygen character orbitals are more stable than the silicon molecular orbitals, which lie higher in energy and are, therefore, more easily ionised; for Te the reverse is true.

For compound **1** the next set of bands, **C**, are associated with the Si–C ionisations, as expected from Fig. 2. For **2**–**4** an additional band **B** intervenes. The Walsh diagrams, and examination of analogous compounds (Fig. 2), suggest that **B** is comprised of two ionisations associated primarily with Si–Si bonding for these three compounds. The third and fourth orbitals for E = S, Se and Te are shown in Fig. 5(a) and (b) respectively. For S and Se they show E–Si bonding characteristics. For Te localisation on Si is almost complete.

For compound **1** an extra band, **D**, appears at higher IE than the Si–C band **C**. The model **5** lacks Si–C bonds but lying below

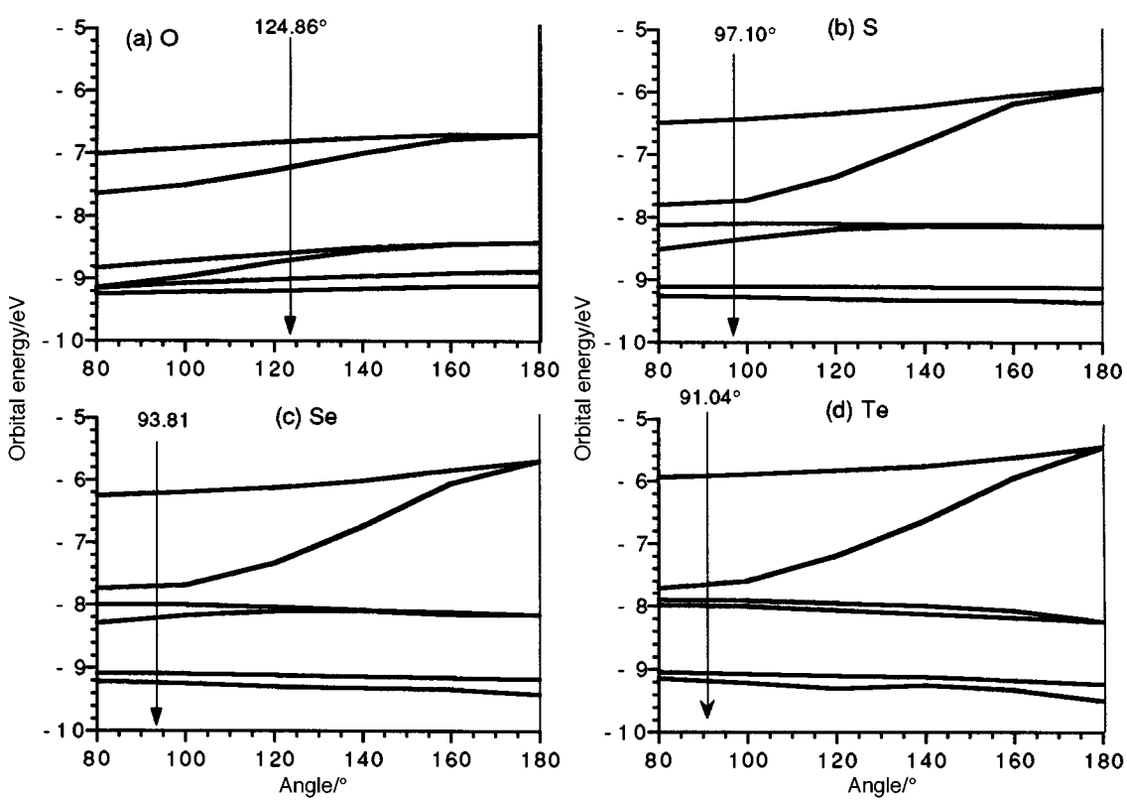

Fig. 3 Diagrams showing the variation in one electron energy of the top six occupied orbitals as a function of H–E–Si angle for compounds **5**–**8**.

Table 3 Optimum H–E–Si angles/° found for compounds **5**–**8** and experimental angles for H_2X

X	$HESi(SiH_3)_3$	H_2E [11]
Oxygen	124.86	104.5
Sulfur	97.10	92
Selenium	93.81	91
Tellurium	91.04	89

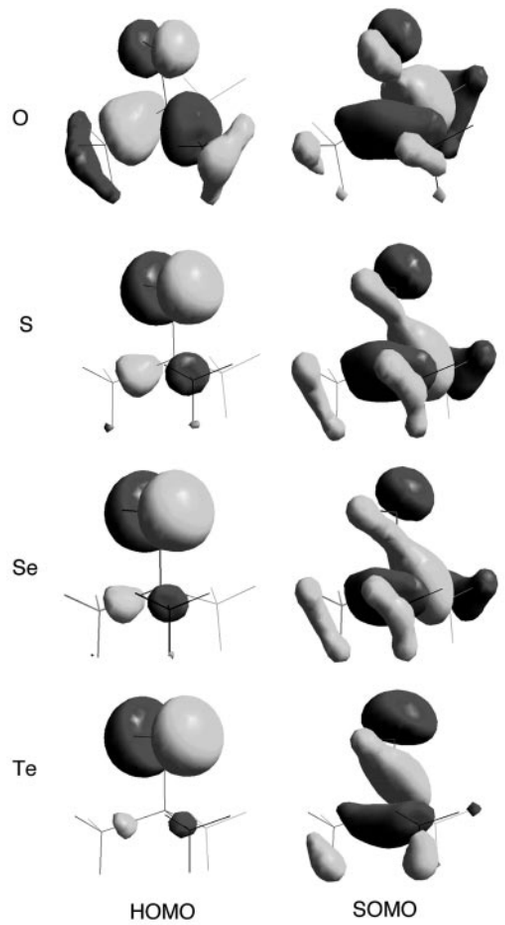

Fig. 4 The frontier orbitals of the chalcogenols found for the geometrically optimised structures of compounds **5**–**8**.

the Si–H set of orbitals are two levels that show similar stabilising O–Si bonding interactions to those discussed above. They are also shown in Fig. 5(a) and (b). Thus band **D** in the spectrum of **1** is assigned to such orbitals, the oxygen character pulling it below the Si–C manifold.

A comparison may also be made between the energy difference between the SOMOs and HOMOs of the chalcogenols, using both the theoretical one electron energy and the difference between peaks **A2** and **A1** seen experimentally. The results are in Table 4. Both the IE differences and the one electron energy differences increase on descending the group, however the former are somewhat greater than the latter. Though, as mentioned above, we are not entitled to expect exact agreement between the differences, it is worth bearing in mind that the absence of methyl groups in the models used for the calculations will have more effect on the one electron energies of the Si–Si bonds than on the chalcogen p orbitals. Thus, if we were to include methyl groups in the calculations we might expect a decrease in the separation of the one electron energies for S, Se and Te.

The change in nature of the HOMO suggests that the site for electrophilic attack on the chalcogenols may well vary as we descend the group. In the alcohol the Si–Si bonds are most vulnerable, but the tellurol, with a completely different type of

Table 4 Comparison of the energy difference found between the IE of bands **A2** and **A1** and the energy separation of SOMO and HOMO by DFT

Chalcogen	Δ One electron energy/eV	Δ Ionisation energy/eV
Oxygen	0.395	<0.300
Sulfur	1.416	0.564
Selenium	1.652	0.717
Tellurium	1.827	>1.00

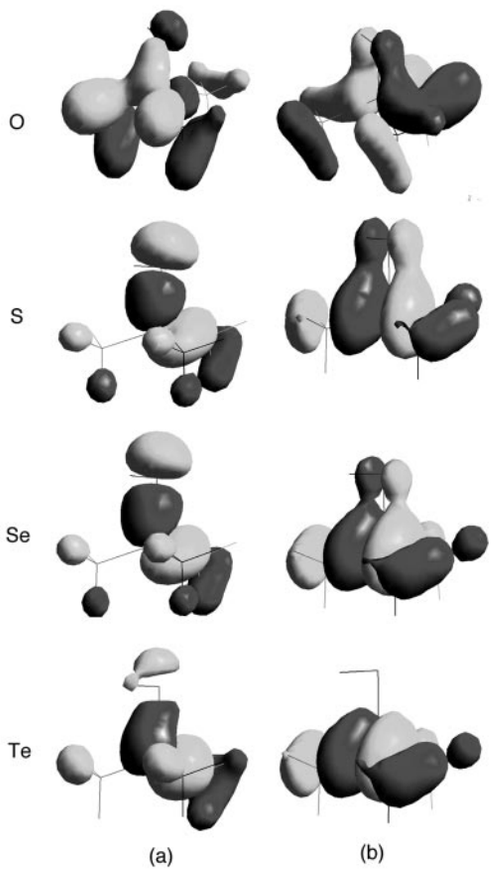

Fig. 5 Representation of the orbitals in $HESi(SiMe_3)_3$ which lead to the observed bands **B** and **D** in the He I photoelectron spectrum.

frontier orbital, may be vulnerable to attack on the chalcogen itself and thus cleavage of Te–H or Te–Si is most likely. Experimental evidence supporting this hypothesis comes from the observation that the tellurol forms H_2Te and the selenol forms H_2Se upon treatment with weak acids but the alcohol is unaffected even by strong acids.

The calculations described above also quantify the postulate described by Christou and Arnold[29] in their studies on the monomeric terminal selenides and tellurides of early transition metals from chalcogenate precursors. They ascribed the facile cleavage of the E–Si bond in the ligand to localisation of the ligand electron density on the chalcogen. Our calculations confirm this hypothesis for the heavier chalcogenides and also provide a possible explanation for the absence of reported examples of similar reactions for the lighter chalcogenides. For these ligands the HOMO is located more in the region of the Si–Si bond.

Conclusion

The photoelectron spectra of a homologous series of chalcogenols have been recorded and modelled using DFT calculations. The unambiguous assignment of the bands in the photoelectron spectra reveals that the HOMO is a π-type orbital whose distribution in the molecule changes as the atomic num-

ber, Z, increases. Thus, the HOMO of the silanol is located on the silicon atoms, and, as Z increases, the HOMO becomes increasingly centred on the chalcogen, such that the HOMO of the tellurol is located entirely on the chalcogen atom. Similarly, as Z increases, the SOMO becomes increasingly centred on the chalcogen. Ionisation energies decrease monotonically as Z increases in accordance with the concomitant reduction of electronegativity and increasingly diffuse orbitals.

The Walsh diagram for $HESi(SiH_3)_3$ (E = O, S, Se or Te) is more complicated than that for H_2E due to mixing of the silicon orbitals with the important chalcogen bonding orbitals, but the same general trend of larger H–E–Si bond angle with increasing Z is observed indicating that the bond angle is dependent on electronic factors rather than steric constraints.

These results go some way to explaining the chemical behaviour of the tris(trimethylsilyl)silyl chalcogenolate complexes and in particular the postulated bond polarisation and location of the HOMO on the tellurium atom partially explains the propensity of the $TeSi(SiMe_3)_3$ ligand to undergo facile Te–Si bond cleavage to form stable terminal telluride complexes.

References

1 J. Arnold, *Prog. Inorg. Chem.*, 1996, **43**, 353.
2 U. Siemeling, *Angew. Chem., Int. Ed. Engl.*, 1993, **32**, 67.
3 R. C. Mehrotra, *Adv. Inorg. Chem. Radiochem.*, 1983, **26**, 269.
4 R. C. Mehrotra, A. Singh and U. M. Tripathi, *Chem. Rev.*, 1991, **91**, 1287.
5 I. P. R. Rothwell and M. H. Chisholm, in *Comprehensive Coordination Chemistry*, eds. G. Wilkinson, R. D. Gillard and J. A. McCleverty, Pergamon, Oxford, 1987, vol. 2, p. 370.
6 I. P. Rothwell, *Acc. Chem. Res.*, 1988, **21**, 153.
7 D. C. Bradley, R. C. Mehrotra and D. P. Gaur, *Metal Alkoxides*, Academic Press, New York, 1978.
8 J. R. Dilworth and J. Hu, *Adv. Inorg. Chem.*, 1993, **40**, 411.
9 H. J. Gysling, *Coord. Chem. Rev.*, 1982, **42**, 133.
10 H. J. Gysling, in *The Chemistry of Organic Selenium and Tellurium Compounds*, Wiley, New York, 1986, p. 679.
11 F. J. Berry, in *Comprehensive Coordination Chemistry*, eds. G. Wilkinson, R. D. Gillard and J. A. McCleverty, Pergamon, Oxford, 1987, vol. 2, p. 661.
12 S. P. Wuller, A. L. Seligson, G. P. Mitchell and J. Arnold, *Inorg. Chem.*, 1995, **34**, 4854.
13 A. L. Seligson and J. Arnold, *J. Am. Chem. Soc.*, 1993, **115**, 8214.
14 D. E. Gindelberger and J. Arnold, *J. Am. Chem. Soc.*, 1992, **114**, 6242.
15 D. E. Gindleberger and J. Arnold, *Inorg. Chem.*, 1994, **33**, 6293.
16 V. Christou and J. Arnold, *J. Am. Chem. Soc.*, 1992, **114**, 6240.
17 V. Christou, S. Wuller and J. Arnold, *J. Am. Chem. Soc.*, 1993, **115**, 10545.
18 C. P. Gerlach, V. Christou and J. Arnold, *Inorg. Chem.*, 1996, **35**, 2758.
19 D. E. Gindleberger and J. Arnold, *Inorg. Chem.*, 1993, **32**, 5813.
20 P. J. Bonasia, D. E. Gindleberger and J. Arnold, *Inorg. Chem.*, 1993, **32**, 5126.
21 P. J. Bonasia and J. Arnold, *J. Am. Chem. Soc.*, 1992, **31**, 2508.
22 C. P. Gerlach and J. Arnold, *Inorg. Chem.*, 1996, **35**, 5770.
23 C. P. Gerlach, S. P. Wuller and J. Arnold, *Chem. Commun.*, 1996, 2565.
24 D. R. Cary and J. Arnold, *J. Am. Chem. Soc.*, 1993, **115**, 2520.
25 D. R. Cary and J. Arnold, *Inorg. Chem.*, 1994, **33**, 1791.
26 D. R. Cary, G. E. Ball and J. Arnold, *J. Am. Chem. Soc.*, 1995, **117**, 3492.
27 B. O. Dabbousi, P. J. Bonasia and J. Arnold, *J. Am. Chem. Soc.*, 1991, **113**, 3186.
28 P. J. Bonasia, D. E. Gindelberger, B. O. Dabbousi and J. Arnold, *J. Am. Chem. Soc.*, 1992, **114**, 5209.
29 V. Christou and J. Arnold, *Angew. Chem., Int. Ed. Engl.*, 1993, **32**, 1450.
30 M. L. Steigerwald and C. R. Sprinkle, *J. Am. Chem. Soc.*, 1987, **109**, 7200.
31 P. O'Brien, *Chemtronics*, 1995, **5**, 61.
32 P. J. Bonasia, V. Christou and J. Arnold, *J. Am. Chem. Soc.*, 1993, **115**, 6777.
33 H. Gilman and R. L. Hanell, *J. Organomet. Chem.*, 1966, **5**, 199.
34 GAUSSIAN 94 (Revision A.1), M. J. Frisch, G. W. Trucks, H. B. Schlegel, P. M. W. Gill, B. G. Johnson, M. A. Robb, J. R. Cheeseman, T. A. Keith, G. A. Petersson, J. A. Montgomery, K. Ragavachari, M. A. Al-Laham, V. G. Zakrewski, J. V. Ortiz, J. B. Foresman, J. Ciolowski, B. B. Stefanov, A. Nanayakkara, M. Challacombe, C. Y. Peng, P. Y. Ayala, W. Chen, M. W. Wong, J. L. Andres, E. S. Repolge, R. Gomperts, R. L. Martin, D. J. Fox, J. S. Binkley, D. J. Defrees, J. Baker, J. P. Stewart, M. Head-Gordon, C. Gonzalez and J. A. Pople, Gaussian Inc., Pittsburgh, PA, 1995.
35 A. D. Becke, *Phys. Rev. A*, 1988, **38**, 2398.
36 J. C. Slater, *Quantum Theory of Molecules and Solids*, McGraw-Hill, New York, 1974, vol. 4.
37 C. Lee, W. Yang and R. G. Parr, *Phys. Rev. B*, 1988, **37**, 785.
38 S. H. Vosko, L. Wilk and M. Nusair, *Can. J. Phys.*, 1980, **58**, 1200.
39 A. D. Becke, *J. Chem. Phys.*, 1993, **98**, 5648.
40 S. Evans, J. C. Green, P. Joachim and A. Orchard, *J. Chem. Soc., Faraday Trans.*, 1972, 905.
41 A. W. Potts and W. C. Price, *Proc. R. Soc. London, Ser. A*, 1972, **326**, 181.
42 H. Bock and W. Ensslin, *Angew. Chem., Int. Ed. Engl.*, 1972, **10**, 404.
43 H. Bock, P. Mollere, G. Becker and G. Fritz, *J. Organomet. Chem.*, 1973, **61**, 127.
44 H. Bock, P. Mollere, G. Becker and G. Fritz, *J. Organomet. Chem.*, 1973, **61**, 113.
45 R. Boschi, M. F. Lappert, W. Schmidt and B. Wilkins, *J. Organomet. Chem.*, 1973, **50**, 69.
46 R. Parr and W. Yang, in *The International Series of Monographs on Chemistry*, Oxford Science Publications, Oxford, 1989, p. 142.

Paper 8/07070I